

**Response to**

**Second Request for Additional Information – ANP-10286P**

**“U.S. EPR Rod Ejection Accident Methodology Topical Report”**

**Response to Second Request for Additional Information – ANP-10286P  
“U.S. EPR Rod Ejection Accident methodology Topical Report”**

**RAI-3.** *Section 2.1.1 – Please provide the basis (e.g. experimental, mechanistic, etc.) for the oxide buildup model referred to in the report.*

**Response to RAI-3:**

The corrosion calibration database is described in Section 8.1.3.2 of BAW-10231PA, COPERNIC Fuel Rod Design Computer Code (Topical Report Reference 2). A comparison plot of measured and predicted is provided in BAW-10231PA, Figure 8-15. BAW-10231PA, Figure 8-16 provides the oxide thickness as a function of rod average burnup. For hydriding, an experimental validation is given in Section 8.2.3.2, Figure 8-26, and Figure 8-27 of BAW-10231PA. The maximum corrosion layer thickness of 35  $\mu\text{m}$  referenced in Topical Report (TR) Section 2.1.1 was predicted from the maximum burnup point of the fuel rod performance evaluation under an enveloping power history.

**RAI-4.** *Section 2.3 – Please provide a more detailed discussion concerning TFGR and FGRF*

**Response to RAI-4:**

Conformance with Standard Review Plan (SRP) 4.2 (TR Reference 1), regarding radiological fission gas release (FGR) dependence on prompt fuel enthalpy dependence, requires a coupling between fuel failures, local energy depositions, and radiological releases. TFGR is the Transient FGR expression from SRP 4.2, Appendix B, Section D. The number of pins that fail due to exceeding the DNBR limit, F, is predicted from the NEMO-K neutronics and LYNXT thermal hydraulics calculations. The maximum allowed number of fuel rods that can fail due only to departure from nucleate boiling ratio (DNBR) failures, A, is determined by radiological consequence calculations in accordance with Regulatory Guide 1.183 and SRP 15.0.3. This analysis has a percent of fission gas release from the pellets specified to determine the radiological inventory of a particular pin to determine the dose from the release. From a dose calculation for a DNBR failure, a correlation can be made between the dose from additional TFGR and a DNBR failure. The correlation is used to determine the equivalent number of additional rods to be considered failed, FGRF. The equivalent total number of fuel rods failed (EQP) is the sum of those failed due to DNBR, F, and the equivalent number of additional rods due to the TFGR.

For example, if the base release inventory for a fuel rod failure exceeding DNBR is 10 percent FGR and the enthalpy rise of the pin yields a TFGR of 5 percent, then for this fuel rod, the total fission gas release would be 15 percent. This amount of release is equivalent to 1.5 failures for the value of EQP for this pin rather than 1.0. This calculation would be repeated for all fuel rods that have an enthalpy rise greater than 31.2  $\Delta\text{cal/g}$ . The sum of the individual rod EQPs is then compared against the value of A. For the U.S. EPR, the maximum number of equivalent failures is 30 percent of the core (i.e., 19,159 fuel rods) and no additional fuel failures needed to be considered because the peak enthalpy rise for all the rod ejection cases was less than 31.2  $\Delta\text{cal/g}$ .

**RAI-5.** Section 4.1.4 – (Table 4-1) The knowledge ratio (KR) for fuel feedback is given as 96. Doppler feedback is generally  $\pm 10$  percent at best. Please explain how the uncertainty in the DTC is determined throughout the burnup range?

**Response to RAI-5:**

A 10 percent uncertainty was determined based on the underprediction of the Doppler Power Coefficients (DPC) compared to measurements. Table 5-1 lists the DPC predictions to measurements for NEMO from the NEMO computer code in BAW-10180A-01, NEMO – Nodal Expansion Method Optimized (Reference 1) and for NEMO using the fuel temperature model with  $T_{eff}$  in TR Section 6.2.4. The predictions of these models underestimate the measured magnitude of the DPC by approximately 20 percent with either model. The DPC is proportional to the Doppler Temperature Coefficient (DTC) with the proportional constant being the ratio of the fuel temperature change to the percent power change. The bias could be from either the DTC or the fuel temperature predictions. These benchmarks are performed at beginning of cycle (BOC) for a cycle 1 core which has less than 6 EFPD of irradiation. Because the fuel properties for fuel with zero burnup are well characterized, it is unlikely that every pin in the core is biased low in the fuel temperature predictions. Therefore, a significant portion of underprediction in the DPC magnitude is probably due to the DTC component of the DPC. Having a lower prediction for the magnitude of the DTC is conservative for the ejected rod application due to a resultant lower negative reactivity feedback. Due to this conservatism and the 10 percent additional uncertainty, sufficient conservatism exists in the model, and no additional penalty was assessed as a function of burnup.

**Table 5-1—Doppler Power Coefficient Comparisons to Measured**

Power Level, %	Measured DPC, pcm/%full power	NEMO with TACO3 Average Fuel Temperature DPC (% Difference $\{(M-P)/M*100\}$ )	NEMO with COPERNIC dynamic fuel rod model and Teff DPC (% Difference $\{(M-P)/M*100\}$ )
30	-13.6	-11.1 (-18%)	[ ]
50	-12.7	-10.4 (-18%)	[ ]
75	-11.6	-9.2 (-21%)	[ ]

**References for RAI-5:**

1. BAW-10180A-01, NEMO – Nodal Expansion Method Optimized, Revision 1, July 1993.

**RAI-6.** Table 4-1 – Please explain what method is used to determine  $\beta_{eff}$  and the associated uncertainty.

**Response to RAI-6:**

The method to calculate the core average  $\beta_{eff}$  is the sum of the beta fractions for each of the major fissionable isotopes (i.e., U-235, U-238, Pu-239, Pu-241) weighted by the respective fission rates for each simulator node. An effectiveness factor of [ ] is applied. The core average betas are scaled to bound the uncertainty and the amount of excess margin for future designs and these scaled betas are input to NEMO-K to use for the transient. TR Sections

4.1.5 and 7.1.4 provide the rationale for this uncertainty. Also, BAW-10120PA "Comparison of Core Physics Calculations with Measurements," (Reference 1) Section 3.2.3 describes  $\beta_{\text{eff}}$  uncertainties and defines a 5 percent uncertainty for  $\beta_{\text{eff}}$ .

**References for RAI-6:**

1. BAW-10120PA, "Comparison of Core Physics Calculations with Measurements," J. J. Woods et al, July 1979.

**RAI-7.** *Section 4.1.6 – Please elaborate on the last sentence in Section 4.1.6 to explain how and why the sensitivity of the trip reactivity to “at power” events determines the level of conservatism of the trip reactivity.*

**Response to RAI-7:**

The last sentence in Section 4.1.6 is intended to address the importance of trip reactivity for the ejected rod event at power even though the Phenomena Importance Ranking Tables (PIRT) analysis did not rate trip reactivity as an important parameter. The insertion of the rods may affect the timing of the severity of the departure from nucleate boiling (DNB) response as core power decreases. The trip reactivity is evaluated in TR Section 7.1.7, Table 7-3 to illustrate the difference between a nominal control rod worth and the rod worth reduced by 9 percent. The reduced scram rod worth simulates a limiting trippable rod worth by reducing the worth by the uncertainty and excluding the ejected rod. The total rod worth uncertainty reduction is 10 percent for shutdown margin calculations; however, the reactivity worth of the inserted bank from which a rod is ejected is increased by more than 15 percent. The net effect on the total tripped worth was 9 percent for the case studied. The sensitivity case showed only a [ ] percent core power difference at [ ] percent power. Since the sensitivity is small to trippable worth and the slightly higher power results in a conservative estimate of DNBR, the ejected rod model uses an approximate 10% worth reduction of the remaining banks to be tripped.

**RAI-8.** *Section 4.1.10 – Please clarify whether there is a provision to account for direct heating of the coolant due to the increase in neutron and gamma ray flux during the transient.*

**Response to RAI-8:**

The provision to account for direct heating of the coolant is made by depositing into the coolant a fraction of the total power produced. For the U.S. EPR, the fractional heat deposited in the coolant was 2.6 percent of the total power produced. Because this fraction is applied to the power produced with time, the power deposited in the water is proportional to the transient power produced by the pin. This direct heating provision is included in both the NEMO-K and LYNXT simulations.

**RAI-9.** *Section 4.2.8 – When MDNBR is exceeded, the topical report stated that static heat transfer, CHF, and failure are conservatively assumed. Please provide justification for this position.*

**Response to RAI-9:**

BAW-10156A (TR Reference 7) addresses a CHF correlation developed from static testing in transient heat transfer analyses. Appendix G of BAW-10156A provides the response to an RAI and justification for performing transient CHF evaluations with transient system boundary conditions and steady-state CHF correlations. BAW-10156A, Appendix Section B.4 (Heat Transfer Correlations) and Appendix pages D-3 through D-6 (logic for selecting the heat transfer mode) provide descriptions of the heat transfer package implemented into the LYNXT computer code.

**RAI-10.** *Section 6.2.1 – Please clarify whether the lead time constant and the lagged signal time constant are consistent with the reactor design. Provide their respective values.*

**Response to RAI-10:**

TR Table 8-1 provides the values for the analysis for the lag rate constant and the gain constant. The gain constant is another name for the derivative lead time constant defined in the signal filter equation in TR Section 6.2.1.2. The values used in the sample calculations are both 30 seconds and are specified as inputs for reactor safety analysis. Any modifications to the signal parameter values based on actual circuitry design or implementation will be evaluated for impact on the analysis as indicated in Note b to the ejected rod analysis checklist in TR Table 9-1. A small sensitivity to these constants is shown in the response to question RAI-29 for transients with power changes occurring for less than a second.

**RAI-11.** *Section 6.2.3 – Please provide a typical magnitude of the adjustment factors used in sensitivity analyses.*

**Response to RAI-11:**

The result of using the adjustment factors in TR Section 6.2.3 that are used in the sensitivity analysis in TR Section 7.1.7 are shown in TR Table 7-3 in terms of percent change. For fuel conductivity and gap conductance, the relationship between adjustment factors and the uncertainty is given by the equation  $(100 + \% \text{ uncertainty})/100$ . Because the Doppler coefficient and the rod worth are calculated values by the code, the adjustment factors on the cross sections for Doppler and rod worth require an iteration process to obtain the target percent difference. The equation is an approximation to serve as the initialization point for the iteration process for these factors.

**RAI-12.** *Section 6.2.4 – Does NEMO-K calculate the temperatures, or are they calculated by LYNXT and passed to NEMO-K? If they are passed to NEMO-K, is the connection a dynamic one? Has the relationship developed for  $T_{eff}$  been validated against another method? If another method has been used, please describe it and discuss the accuracy of that method.*

**Response to RAI-12:**

NEMO-K calculates a dynamic fuel temperature using a 1D concentric radial ring fuel rod model as described in BAW-10221PA (TR Reference 6) and is not dependent upon LYNXT for its fuel and moderator temperature calculations. Both NEMO-K and LYNXT use COPERNIC based fuel and clad properties and both use the same gap conductivity model. The fraction of core power and power distribution versus time from NEMO-K are passed to LYNXT.

The relationship for T-effective temperature ( $T_{eff}$ ) has been validated with the computer code APOLLO2 described in BAW-10228PA, (Reference 1). The reactivity and U-238 capture rate of several snapshot fuel temperature distributions at steady state conditions and those temperatures expected during a Reactivity Initiated Accident (RIA) event were examined with APOLLO2. Calculations were repeated with a uniform fuel temperature until the reactivity and U-238 capture rates were equivalent to the non-uniform temperature distributions. This uniform temperature was defined as the effective temperature and compared to the values predicted by Rowland's formula and the new  $T_{eff}$  formula. Fifteen cases were run for each temperature distribution, which spanned burnups from 0 to 60 GWD/MTU and U-235 enrichments from [ ] weight percent (w/o). Results showed that Rowland's formula resulted in nearly the same temperature as the new  $T_{eff}$  formula for steady state cases, and that both agreed with the APOLLO2 effective temperature. For the transient fuel temperature cases, the new  $T_{eff}$  definition showed substantial improvement reducing the mean prediction error of  $T_{eff}$  from a range [ ] K for the Rowlands formula down to a range of [ ] K. Both models had about a [ ] K standard deviation. The APOLLO2 temperature solution was benchmarked to Monte Carlo N-Particle (MCNP) transport code calculations. In addition, the  $T_{eff}$  method was compared in TR Table 7-3 to an average temperature formulation and was found to yield slightly more limiting results than a simple average weighting.

**References for RAI-12:**

1. BAW-10228PA, "Science," Framatome Cogema Fuels, December 2000.

**RAI-13.** *Section 6.3.2 – Is there a case in which the power profile within the pellet changes during the transient? If there is no provision for this change in profile, what is the effect of not allowing the change?*

**Response to RAI-13:**

The radial power profile does not change during the transient. The conditions that do change during a transient do not affect the radial power profile. The pellet radial power profile is primarily a function of burnup and initial enrichment. These two conditions are not affected by transient behavior. The burnup determines the amount of plutonium created in the rim of the pellet from U-238 resonance absorptions. At high burnups, the rim power can be twice as high as the average pellet power. The initial enrichment also has an effect, but it is less pronounced.

Initially, the higher enrichment has a slightly higher surface power because of the higher self shielding of thermal flux. As the plutonium is created on the rim, the plutonium power fraction is less in a higher enrichment pellet, and the surface power is smaller than a lower enriched pellet at the same burnup. The initial enrichment and burnup for the pellet are initial conditions for the transient and the pellet radial power profile remains fixed during the transient. A sensitivity study was performed on the neutronics solution assuming all the fuel was 2.0 w/o fuel and 5.0 w/o fuel with little or no sensitivity to the NEMO-K results (see TR Table 7-3).

**RAI-14.** *Section 6.3.3.1 – The CG/TDP model was validated for BOL conditions against various methods. Has this same validation also been carried out for EOL conditions, or is the validation at EOL conditions limited to only a comparison with COPERNIC?*

**Response to RAI-14:**

The purpose of the validation calculations at BOL conditions was to demonstrate continuity to existing results in Section 6.2.2 of BAW-10156A (TR Reference 7) and that the LYNXT fuel rod model remains valid for predicting fuel temperatures with each of the fuel options. No additional comparisons of LYNXT to LYNXT model option were performed for end of life (EOL) conditions. The BOL and EOL comparisons were made only for different transients with LYNXT and COPERNIC in order to show that the CG/TDP model provides similar results to the COPERNIC detailed model.

**RAI-15.** *Section 6.3.3.2 – Table 6-3 summarizes the comparison between LYNXT and COPERNIC. Please elaborate on how the results are determined.*

**Response to RAI-15:**

At each common time point in the two computer code simulations, the ratio of the respective fuel and cladding temperature results from the two codes is calculated. The ratio is the COPERNIC result divided by the LYNXT Constant Gap/Temperature Dependent Property (CG/TDP) result. For each of the four transients (hot zero power (HZIP) EOL, hot full power (HFP) EOL, HZIP beginning of life (BOL), and HFP BOL), the average, standard deviation, maximum, and minimum of the ratios during the transient simulation are calculated and tabulated in TR Table 6-3. The sample size reported in TR Table 6-3 is the number of common time points during the transient.

A revision to TR Table 6-3 was made as part of the response to RAI-31. The marked-up TR Table 6-3 is attached to this RAI response.

**RAI-16.** *Section 6.3.4 – Is there a standard set of data for the thermal properties of the fuel and clad, gap conductance, and radial power profile that are used as input to these analyses, or are they calculated as needed by one of the detail codes? If there is a standard set please list them or give appropriate references.*

**Response to RAI-16:**

The thermal properties are a standard set for the fuel rod design generated by using fuel and clad thermal property correlations in BAW-10231PA (TR Reference 2). A set of tables as a

function of temperature at a particular fuel rod burnup are input to LYNXT. These tables are available for different fuel pellet initial porosities, U-235 enrichments, and gadolinia content. Table 16-1, Table 16-2, and Table 16-3 provide a representative set for the fuel rod material compositions and burnups considered for the sample calculations in the topical report. Each fuel rod design can have a set of properties used for finer detail and response or a set of constant values can be used. NEMO-K uses the correlations in the form of the BAW-10231PA equations.

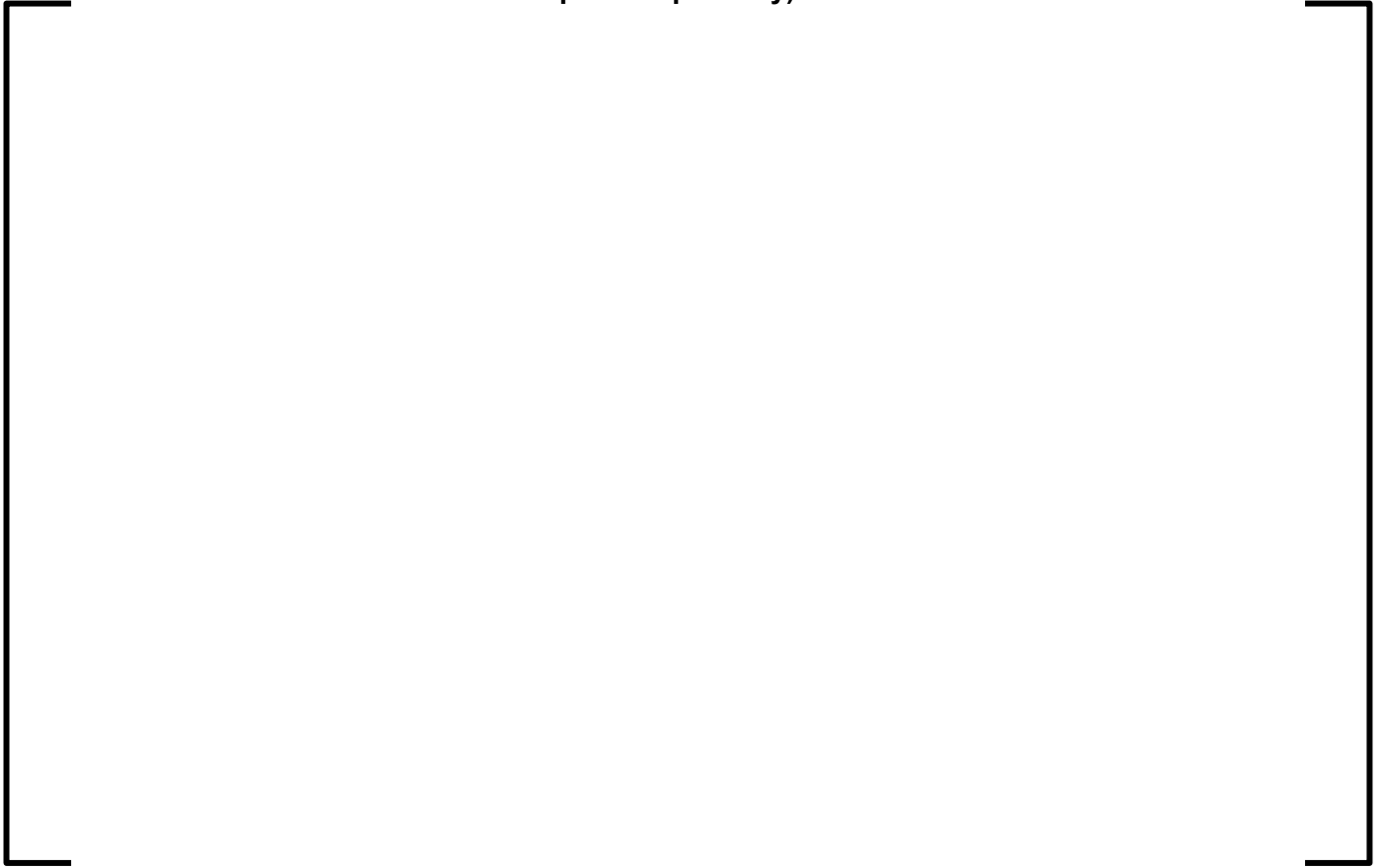
The fuel rod to cladding gas gap conductance (HGAP) used in the TR sample problem are given in Table 16-4. The HGAP is represented as a [ ] used as index interpolation points for HGAP. The [ ] index points for the TR sample problem calculations are [ ]. The [ ] index points for the TR sample problem calculations are [ ]. Both LYNXT and NEMO-K use a tabular input for this property.

The fuel pellet radial power profile used in the TR sample problem calculations consists of an array of normalized power density as a function of normalized radial position. This power profile is enrichment and burnup dependent. The values for UO<sub>2</sub> fuel pellets with [ ] w/o enriched U-235 at various levels of burnup are given in Table 16-5. These values are taken from the standard depletion dependent power profiles provided in the COPERNIC computer code BAW-10231PA. For fuel pellets loaded with gadolinia, the sets of pellet power profiles used for the TR sample problem are provided in Table 16-6 and Table 16-7 for fuel pellets loaded with [ ] w/o and [ ] w/o gadolinia, respectively.

**Table 16-1—Cladding Thermal Properties from COPERNIC Correlations**

A large, empty rectangular frame with a thin black border, centered on the page. It is intended to represent the content of Table 16-1, which is missing from this page.

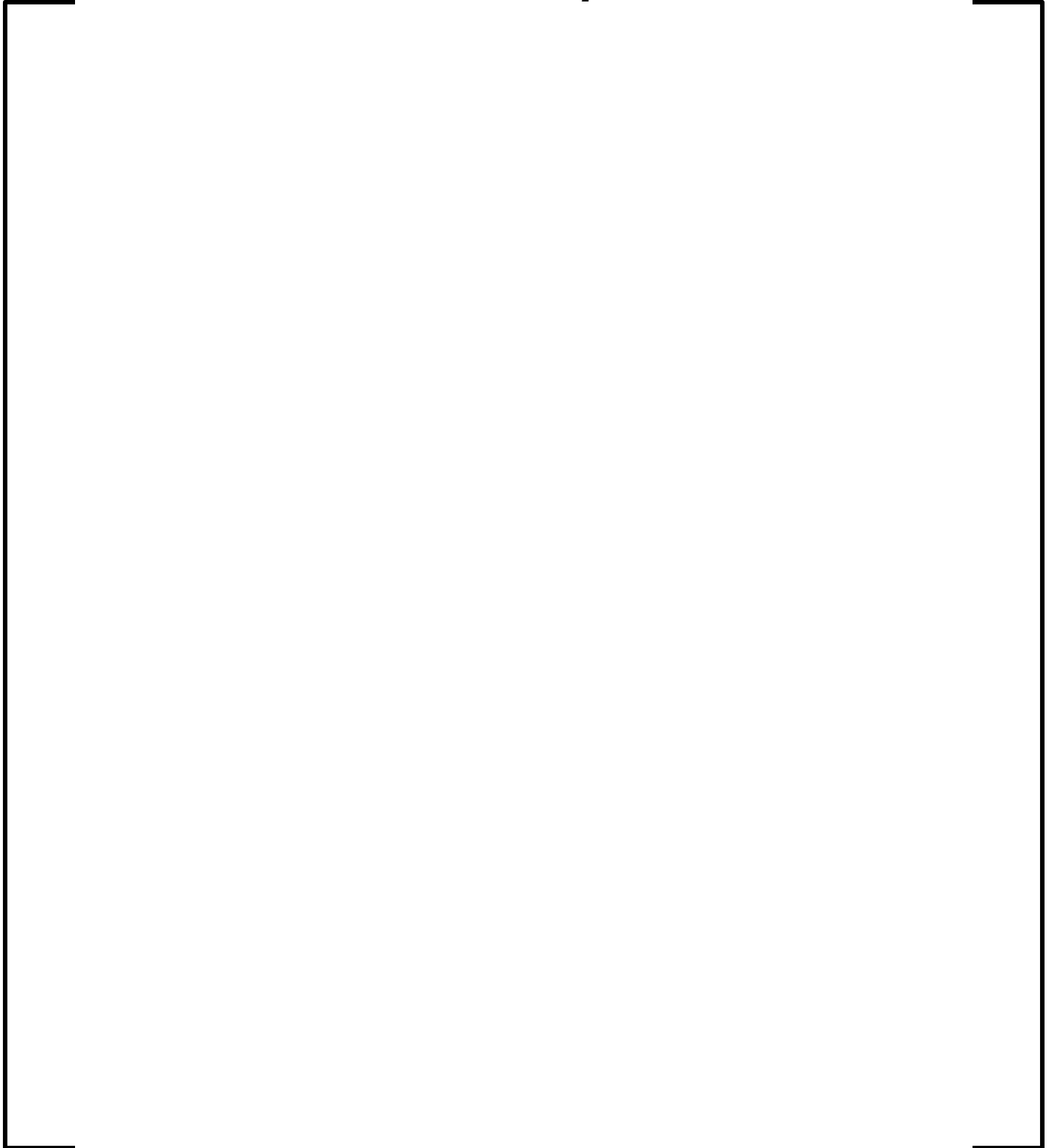
**Table 16-2—UO<sub>2</sub> Fuel Thermal Properties from COPERNIC Correlations (4 percent porosity)**

A large, empty rectangular frame with a black border, positioned centrally on the page. It is intended to contain the data for Table 16-2, but the content is missing.

**Table 16-3—Gadolinia Fuel Thermal Properties from COPENIC  
Correlations at 50 GWd/tU (4 percent porosity)**



**Table 16-4—Burnup Dependent Gap Conductance Tables for 5 w/o U-235  
enriched UO<sub>2</sub>**

A large, empty rectangular frame with a black border, occupying most of the page below the caption. It appears to be a placeholder for a table that is not present in this version of the document.

**Table 16-5—Pellet Radial Power Profile for UO<sub>2</sub> with 5 w/o enriched U-235**



**Table 16-6—Pellet Radial Power Profile for  $\text{UO}_2$ :  $\text{Gd}_2\text{O}_3$  with 4.85 w/o U-235 enriched and 4 w/o gadolinia**

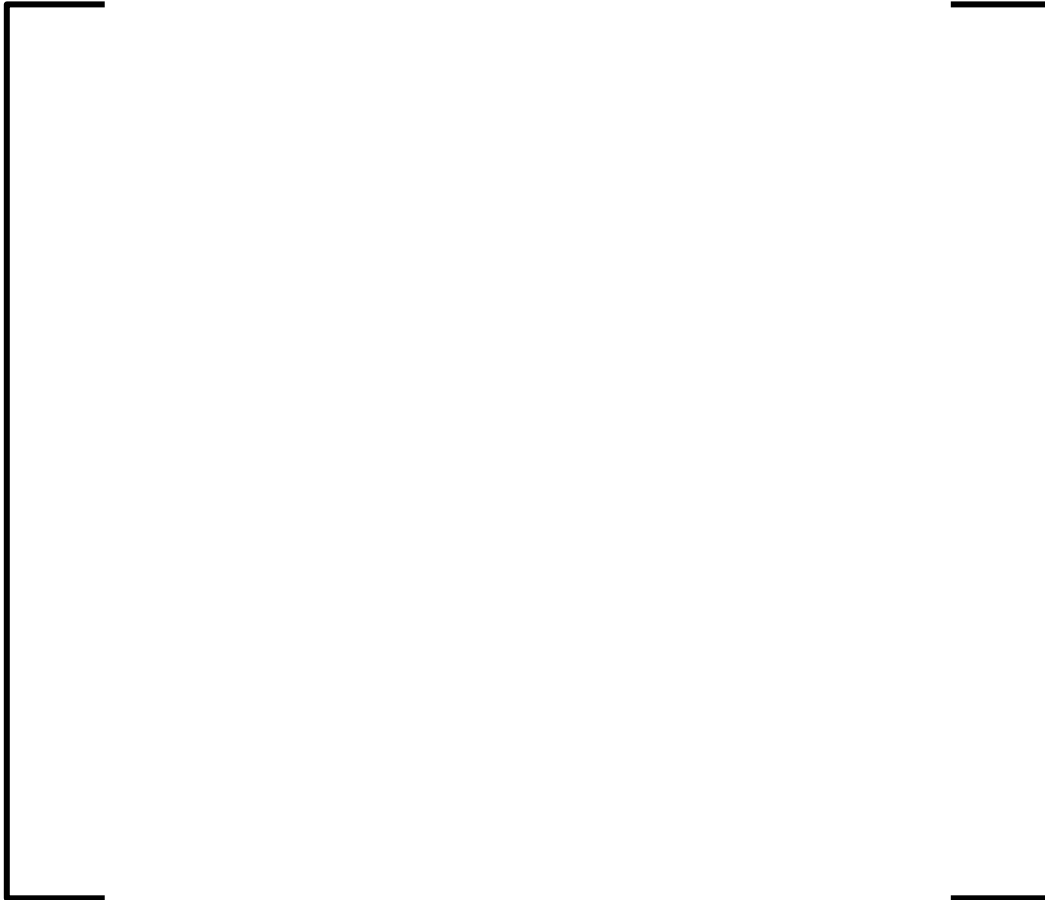
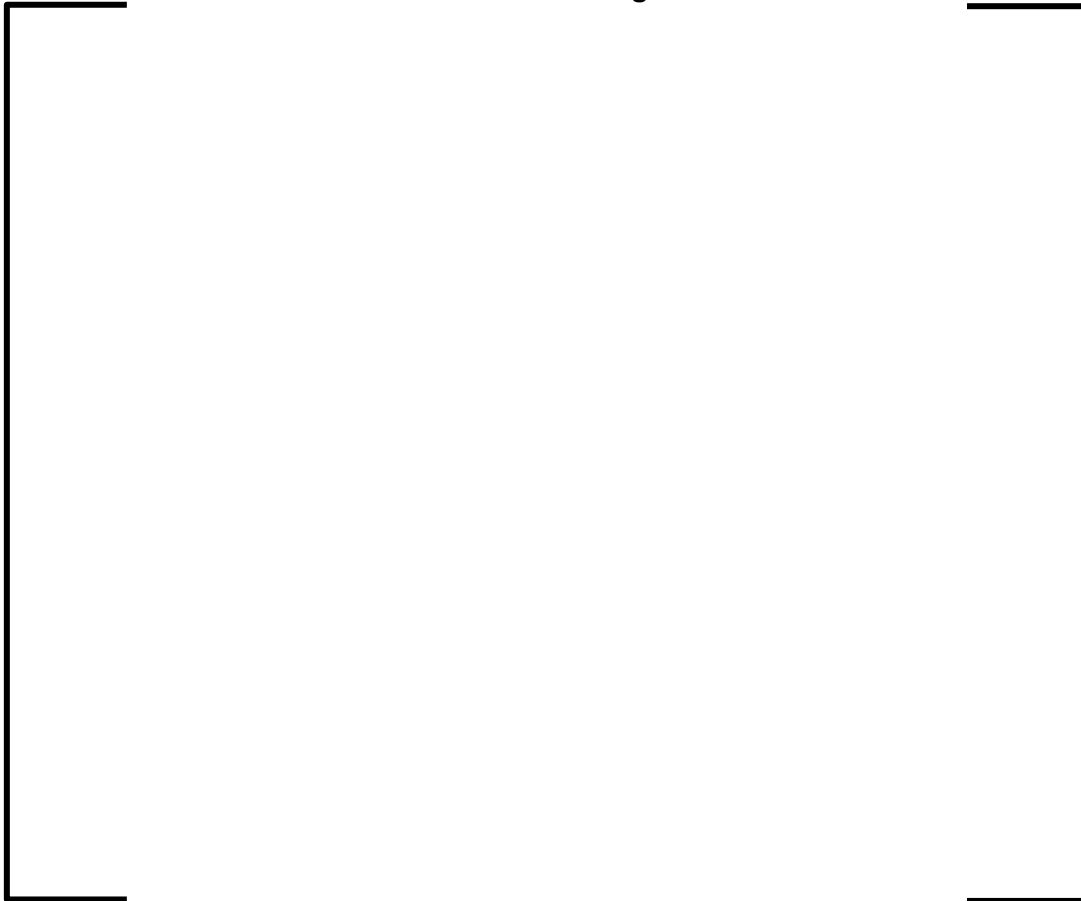


**Table 16-7—Pellet Radial Power Profile for UO<sub>2</sub>: Gd<sub>2</sub>O<sub>3</sub> with 3.57 w/o U-235 enriched and 8 w/o gadolinia**



**RAI-17.** *Section 7.0 – To what do the uncertainties in Table 7-1 refer? REA analysis values seem to be further from PRISM range values than uncertainties. Please provide proper references and explanations.*

**Response to RAI-17:**

The uncertainties referred to in TR Table 7-1 are the uncertainties to be applied to the calculated values from PRISM. The analyzed value should always be greater than the PRISM value with the uncertainty applied. The purpose of TR Table 7-1 is to show the difference between nominal value at the insertion limit and the REA analysis value. The amount between the PRISM calculated values and the REA analysis value is to account for the uncertainty, abnormal xenon distribution, and extra conservatism that can be used for future design margin. For example, the BOC Cycle 1 calculated ejected rod reactivity worth was 180 percent milli- $\Delta k/k$  (pcm). At adverse xenon conditions, the ejected worth became 291 pcm and increasing it by 15 percent results in a value of 335 pcm. This latter value is included in TR Table 9-2. The difference between 335 pcm and the REA analysis value of 433 pcm is amount of margin between this cycle and the analysis limit for this parameter.

**RAI-18.** *Section 7.1.3 – Is the value DTC uncertainty of  $\pm 10$  percent equally valid for BOL and EOL conditions? Please explain its burn-up dependency.*

**Response to RAI-18:**

The uncertainty of  $\pm 10$  percent is equally valid for all burnup conditions. Because U-238 dominates the Doppler temperature effect and the concentration of U-238 does not vary significantly with burnup, the same uncertainty value for BOC and EOC is appropriate. The Doppler temperature coefficient becomes more negative with burnup as Pu-240 is created. The DTC difference from BOC to EOC of Cycle 1 is approximately a [ ] percent increase in magnitude, which is indicative of the Pu-240 contribution to DTC. However, even if the error of Doppler contribution of Pu-240 was twice the assumed value of 10 percent, the implied error would increase [ ] percent, which is an insignificant amount relative to the overall conservatism described in the response to RAI-5.

For clarification, in the context of the topical report, the use of the terms BOC and EOC is in reference to burnup point in a particular operating cycle between core reloads. For the topical report, the use of the terms BOL and EOL refer to the operational duty time of a fuel rod, which may stretch over several core operating cycles. The DTC for the topical report is treated as a core wide parameter; therefore, the response in the paragraph above refers to BOC/EOC conditions instead of BOL/EOL conditions.

**RAI-19.** *Section 7.1.7 – Are combinations of the uncertainties listed in Table 7-3 evaluated when performing uncertainty analyses? If so, please explain what combinations are evaluated.*

**Response to RAI-19:**

The sensitivity studies were performed at the conditions listed in TR Table 7-3. When more than one “ $\Delta$  Case Conditions” is listed within a row, all of the listed changes were made in the input to obtain a single output sensitivity for each transient examined.

**RAI-20.** *Section 7.2.1 – Have sensitivity calculations been carried out using different node selections? If so, explain the node sensitivity analysis results.*

**Response to RAI-20:**

The LYNXT radial model nodalization is the same channel geometry as the baseline model used in other MDNBR analyses for the U.S. EPR (e.g., U.S. EPR FSAR Tier 2, Chapter 15 events). This radial geometry is presented in TR Figure 7-8. The axial nodalization used is based on the fuel assembly grid spacer locations and a reduced number of nodes from the baseline model for computational efficiency given the large number of time steps required. No other node selection sensitivity was performed.

**RAI-21.** *Section 7.2.4 – Please clarify whether NEMO-K and LYNXT use the same nodal distribution.*

**Response to RAI-21:**

NEMO-K and LYNXT are independent models; therefore, they are not required to use the same nodal distribution. The axial power shape data passed to LYNXT model input from NEMO-K model output is converted to the axial elevation spacing required by LYNXT. The fuel rod powers supplied to LYNXT from NEMO-K are calculated from the  $F_{\Delta H}$  power transient of the fuel assembly of interest and its neighboring assemblies. The powers are mapped to the LYNXT model geometry with an intra-assembly radial power distribution. This radial power distribution is discussed further in the response to RAI-30.

**RAI-22.** *Section 7.2.5 – In Fig 7-10 the no-gadolinia case does not bound the gadolinia cases over the entire time span, which appears to be contradictory to statements in Section 7.2.5. Please explain this discrepancy.*

**Response to RAI-22:**

While TR Section 7.2.5 states that  $UO_2$  is bounding, it was meant to be bounding in terms of the maximum temperature achieved during the transient, not that the  $UO_2$  fuel temperature was bounding over the gadolinia fuel temperature at every time step.

TR Section 7.2.5, page 7-9 will be revised as follows:

“Note that the fuel temperatures with gadolinia are higher when operating at the same linear heat rate as  $UO_2$ . When the transient temperatures for gadolinia fuel are adjusted by the power reduction factor, the maximum temperature during the transient is bounded by the  $UO_2$  maximum temperature.”

A marked-up TR page 7-9 which reflects this change is attached to this RAI response.

**RAI-23.** *Section 8.5 – Please provide more information as to why no fuel rod failures are reported. For example, is it due to: a reactor trip terminating the transient, negative feedback reversing the trend, thermal inertia in the system reducing the temperatures, all of the above, etc.?*

**Response to RAI-23:**

TR Table 8-3, TR Table 8-4, and TR Table 8-5 summarize the results from the spectrum of rod ejections for a spectrum of initial power levels at BOC and EOC. There are no failures reported for events that tripped on high rate of flux on the excore detectors and that had minimum departure from nucleate boiling ratio (MDNBR) greater than the specified acceptable fuel design limits (SAFDL) during the transient. Therefore, no failures are reported for the BOC 35 percent power, EOC HZP, EOC 25 percent power, and EOC 35 percent power cases. The transient pulse is limited by the Doppler reactivity worth of the fuel rod heat up to counter the ejected rod worth and then ultimately terminated by the reactor scram.

The failed fuel rod census is performed for the transients where the fuel rod conditions reach the MDNBR SAFDL threshold for the potential of fuel failure. None of the cases for the TR sample problem have an enthalpy rise that exceeds 31.2  $\Delta$ cal/gm; therefore, the TFGR augmented fuel failure consideration is not needed. The response to RAI-28 describes the process by which the fuel failure census is completed. As shown in TR Figure 8-20 and Figure 8-35, the MDNBR of the bounding peak fuel rod for the 60 percent power cases only briefly crosses the SAFDL threshold by a small amount. It includes a multiplier on the initial peaking to bound cycle to cycle variations. However, the actual core power distribution that is used for the census only applies the uncertainties with no allowance for cycle to cycle variation and this power distribution did not have any fuel rods with heating rates where the MDNBR is exceeded.

**RAI-24.** *Please list the model assumptions used to generate the LYNXT to COPERNIC transient model comparison.*

**Response to RAI-24:**

The LYNXT to COPERNIC models were designed to investigate the performance of the LYNXT CG/TDP fuel rod model using the tabular fuel thermal properties compared to the COPERNIC full detailed capability model. The modelling assumptions used for the LYNXT to COPERNIC transient model comparison are listed below:

- A model of a single fuel rod with the same pellet radial power profile.
- Uniform power distribution in the axial direction to allow a single axial node to be compared.
- Same power history transient for the fuel. Time dependent inputs for LYNXT were linearly interpolated between no more than 101 input values. COPERNIC uses step values with a significantly finer mesh.
- Constant outer wall cladding temperature (set by creating nearly infinite heat transfer coefficient).
- Fuel pellet mesh—COPERNIC used 5 equal area nodes each with 4 equal area sub-nodes. LYNXT used ten collocation points for twelve radial temperature values.
- Cladding mesh—COPERNIC used 4 equal area nodes. LYNXT used two collocation points.
- Constant burnup profile within the fuel pellet so that fuel rod thermal properties are nearly the same.
- Fuel and cladding thermal properties (conductivity, specific heat, gap conductance)—COPERNIC uses inherent functions of the computer code fuel performance correlations. LYNXT uses tables of properties as a function of temperature (as described in the response to RAI-16).

**RAI-25.** *Supply and describe a flowchart on code and data process linkages that explain the analysis flow path for the REA event.*

**Response to RAI-25:**

A flowchart on code and data process linkages is presented in Figure 25-1.

COPERNIC calculations are run to obtain gap conductivity tables for both NEMO and LYNXT. The fuel property correlation equations from COPERNIC are used in NEMO-K. The fuel property equations from COPERNIC are used to create fitting tables in LYNXT for conductivities and heat capacities for the clad and fuel.

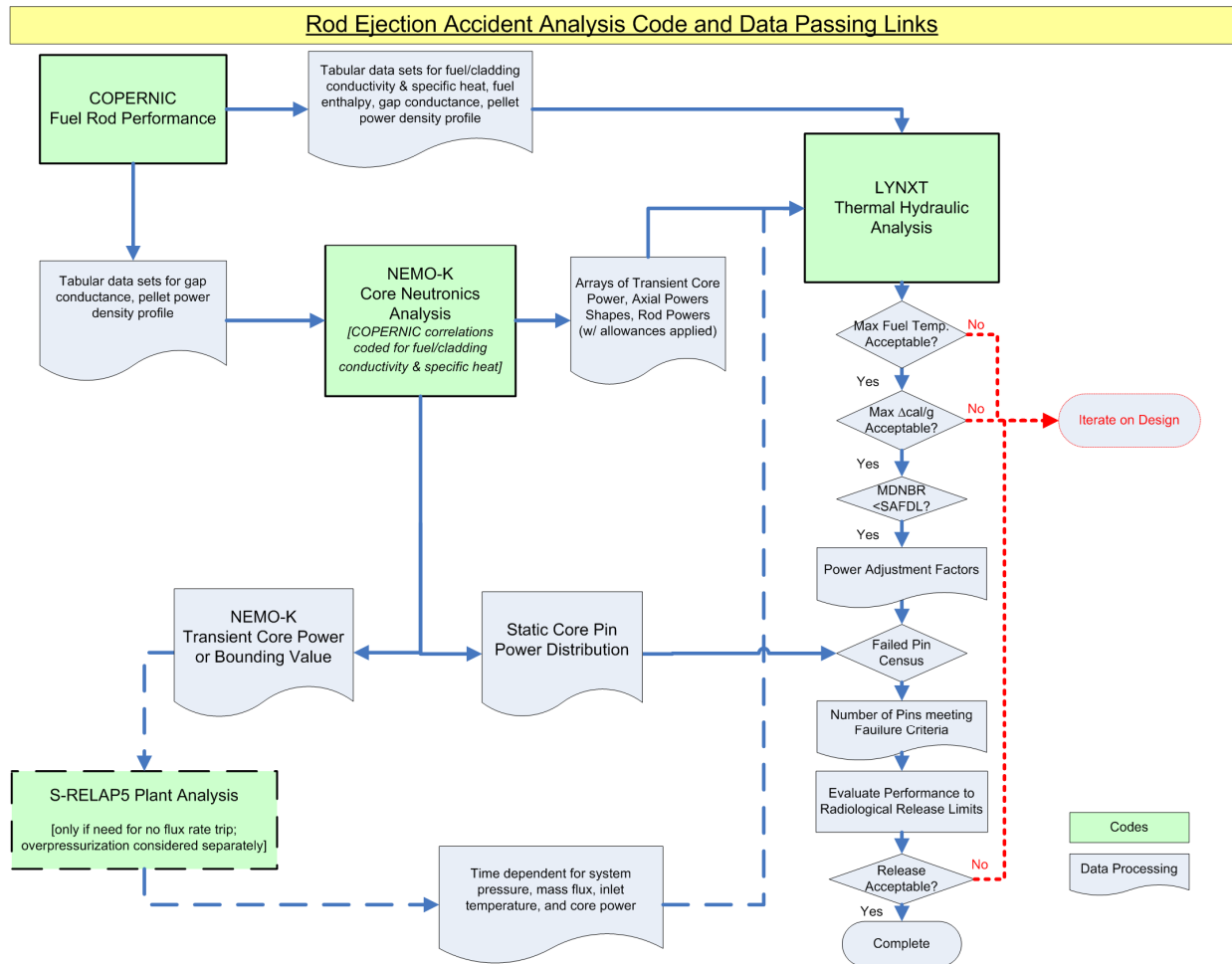
The ejected rod transient is simulated with NEMO-K at each of the plant initial conditions outlined in the topical. The core power,  $F_{\Delta H}$  for the peak pin of interest, and axial powers versus time are extracted from NEMO-K and processed to create inputs for LYNXT.

Two cases (i.e., [ ]) are run with LYNXT for each of the plant conditions as described in the TR Sections 4.2.7 and 7.2.5. The results are reviewed relative to their respective limiting conditions, as discussed in TR Section 2.0 and TR Table 2-1. If the fuel temperature or enthalpy rise is above the SRP 4.2 guidance, the design conditions must be re-evaluated. If these parameters are acceptable at this point, the fuel rod failure census process is followed as described in the response to RAI-28.

If a reactor trip does not occur during the power pulse, both kinetic and static NEMO-K cases are run to bound the power versus time response. This power history information is passed to S-RELAP5 to model the plant system response. The time dependent response of the inlet temperature, flow, and pressure from S-RELAP5 is input to LYNXT to obtain the fuel thermal response for times beyond approximately 5 seconds.

Once the fuel failure census is completed for an iteration of the design, the number of rods is compared against the maximum number of rods that may be failed for radiological release consequences as discussed in TR Section 2.3. If the number of fuel rods considered failed exceeds the limit, the design conditions must be re-evaluated.

**Figure 25-1—Calculation Flow Interfaces**



**RAI-26.** Provide an event timeline and description for various REA events (include events that trip and events that don't trip the plant) to explain the parameter responses. Additionally, please explain the process by which the incore DNBR trip time estimates were made.

**Response to RAI-26:**

An REA event timeline begins with the speed of withdrawal and worth of the ejected rod. The degree of insertion is set by the power dependent insertion limit (PDIL) curve. TR Figure 7-2 depicts the insertion level as a function of power and the extra insertion assumed for the topical report sample problem analysis. For higher powers, only one bank is allowed to be inserted (the "D" bank that includes the N05 and J09 control rod locations). At lower power levels overlap with the "C" bank is allowed, and this is how the total steps is greater than the full travel range of 416 steps.

The minimum time to eject a rod from full insertion was 0.1 second; therefore, for each power level, the time to eject is shortened based on the insertion level of the rod. Table 26-1 provides

the times assumed to eject the rods from various power dependent rod positions for BOC and EOC analysis. Table 26-1 also shows the timing sequence to the peak core fraction of power and the minimum or SAFDL MDNBR values. The first one second of the NEMO-K core power histories for the spectrum of power levels considered at BOC and EOC are presented in Figure 26-1 and Figure 26-2, respectively. Each transient has an initial rapid power rise that is limited by the Doppler reactivity feedback of the fuel rod heat up.

For cases that have reactor trips initiated by the excore flux rate signal, control rods begin to move into the core after an allowance for instrument and signal delays. As shown in TR Table 8-4 and TR Table 8-5, the banks begin insertion between 0.825 and 1.00 seconds for all the rod ejections accidents with the high flux rate trip. The rods are simulated to take 3.5 seconds to become fully inserted after they begin to move. As the rods move in, the axial power distribution shapes and maximum  $F_Q$  values will shift. The changes in the  $F_Q$  appear in the power transient figures, primarily after about 1.5 seconds into the transient due to the time required for the rods to be inserted enough to significantly affect the axial power distribution. The rod ejection accident events that have a trip on the excore neutron signal need no further consideration of the plant boundary conditions because the event is over before the coolant loop transport time has been reached.

As an example of a power history with a reactor trip on high flux rate, an event timeline is provided for the BOC 35 percent power TR sample problem case in Table 26-2.

For transients with no initial excore flux rate reactor trip, further consideration of the event is needed for the fuel rod performance because the plant boundary conditions for inlet temperature, core flow, and system pressure now become more important. As described in TR Sections 6.4 and 8.3, the NEMO-K power transient was provided as input to the S-RELAP5 plant model in order to determine the core thermal performance boundary conditions. A maximum break area was assumed to be the size of the inside diameter or the control rod flange to cause the most rapid depressurization. The BOC 25 percent power, BOC HFP, and EOC HFP transients required the further S-RELAP5 calculations are described in TR Section 8.3.

The system pressure and core inlet temperature for the BOC 25 percent power case are provided in TR Figure 8-12. The transient history of the system pressure, core inlet temperature, core inlet mass flux, and core power normalized to their initial value for this event are shown in Figure 26-3. The transient is terminated at [ ] seconds due to a reactor trip on high S/G pressure. An event timeline of important parameters for this rod ejection transient is provided in Table 26-3. As reported in TR Table 8-3, the predicted number failures with S-RELAP5 plant thermal boundary conditions at the time of the reactor trip was 1.8 percent.

The system pressure and core inlet temperature for the BOC HFP case are provided in TR Figure 8-13. The transient history of the system pressure, core inlet temperature, core inlet mass flux, and core power normalized to their initial value for this event are shown in Figure 26-4. The transient is terminated at [ ] seconds due to a reactor trip on low saturation margin and low primary pressure. An event timeline of the BOC HFP power transient for this rod ejection transient is provided in Table 26-4. For the EOC HFP case, a similar sequence to the BOC HFP case of events is followed.

In addition to the change to the power distribution transient, the DNBR performance is impacted by the decrease in system pressure and the increase in the core inlet temperature increase. A

plot of the pressure versus temperature during this transient is shown in Figure 26-5. The time horizon is such that the upper left corner of the plot (high pressure and low temperature) are the initial conditions and the lower right corner of the plot (low pressure and high temperature) are the conditions at the time of the S RELAP5 predicted reactor trip. The MDNBR resulting from the bounding LYNXT calculations for the BOC HFP case is shown in TR Figure 8-23 and is shown for the EOC HFP case in TR Figure 8-38. The fuel rod failure census is performed (as described in the response to RAI-28) with the final S-RELAP5 boundary conditions and with boundary conditions at several time points leading to the end of the transient. The maximum break area causes the maximum reduction in pressure and the worst boundary conditions for DBNR performance.

The pressure and temperature and a certain fuel rod heating rate can be used as inputs to create a MDNBR response that simulates the DNBR online monitoring system. The online DNBR monitoring system and transient analysis methodology is described in ANP-10287P, "Incore Trip Setpoint and Transient Methodology for U.S. EPR Topical Report," (Reference 1). In Figure 26-5, the two Pressure-Temperature (P-T) threshold lines are estimates of the pressure and temperature conditions required to have MDNBR= [ ] with a fraction of core power of 100 percent and 105 percent. The value to use for the MDNBR threshold was selected for the sample problem calculations as representative of the setpoint threshold that is established in accordance with ANP-10287P. The estimate of Low DNBR reactor trip occurring before 30 seconds is determined by the time just before the P-T crosses the MDNBR= [ ] threshold line for the fraction of power (FOP) equal to 1.00 (P= [ ] psia, T= [ ] °F). The actual time of a reactor trip would be dependent on the size of the break area, the Low DNBR reactor trip setpoint, and the fraction of core power during the event.

**References for RAI 26:**

1. ANP-10287P, Revision 0, "Incore Trip Setpoint and Transient Methodology for U.S. EPR Topical Report," AREVA NP Inc., November 2007.

**Table 26-1—Rod Ejection and Peak Power/MDNBR Times from Spectrum of Power Levels at BOC and EOC**

Initial Power Level (%FP)	RCCA N05 Initial Position (Steps Inserted)	Time to Eject (sec)	Time to Peak Power at BOC (sec)	Time to Limiting MDNBR at BOC (sec)	Time to Peak Power at EOC (sec)	Time to Limiting MDNBR at EOC (sec)
0	411	0.100	N/A	N/A	0.292	0.325 Min
25	411	0.100	0.115	17.0 SAFDL	0.132	0.170 Min
35	384	0.094	0.194	1.10 Min	0.123	0.170 Min
60	308	0.075	0.097	0.74 SAFDL	0.100	0.32 SAFDL
100	140	0.035	0.044	0.99 SAFDL	0.056	0.79 SAFDL

**Table 26-2—Event Timeline for BOC 35 percent Power Transient**

<b>Event</b>	<b>Time (seconds)</b>
Ejection beginning	0.000
Rod N05 fully ejected	0.094
High Neutron Flux Rate of Change Reactor Trip is reached	0.125
Peak Power Reached of 68.7 percent full power	0.194
Safety Bank Scram Rods begin to move	0.850
Minimum MDNBR is reached	1.100
Maximum Peak Fuel Enthalpy Rise is reached	1.350
Maximum Peak Fuel Temperature is reached	1.700

**Table 26-3—Event Timeline for BOC 25 percent Power Transient**

<b>Event</b>	<b>Time (seconds)</b>
Ejection beginning	0.000
Rod N05 Fully Ejected	0.100
Peak Power Reached of 53.1 percent full power	0.469
Core Outlet Temperature rapid rise due to power increase	2.00
Depressurization slows due to core outlet temperature rise	2.00 – 5.00
Core Inlet Temperature begin to rise after flow loop transport	≈9.00
Core Inlet Mass Flux begins to lower due to lower density of coolant	≈9.00
MDNBR reaches SAFLD level	17.00
Reactor Trip Setpoint reached (High S/G Pressure)	24.94
Reactor Trip	25.44
Turbine Trip	26.44
Safety Bank Scram Rods fully inserted	29.34

**Table 26-4—Event Timeline for BOC HFP Power Transient**

<b>Event</b>	<b>Time (seconds)</b>
Ejection beginning	0.000
Rod N05 Fully Ejected	0.035
Peak Power Reached of 110.2 percent full power	0.121
MDNBR reaches SAFDL level	0.900
Peak Cladding Temperature begins Post-CHF transition	1.350
Core Outlet Temperature rapid rise due to power increase	2.00
Depressurization slows due to core outlet temperature rise	2.00 – 5.00
Peak Fuel Average Temperature begins post CHF transition	5.000
Peak Fuel Temperature begins post-CHF transition	9.500
Core Inlet Temperature begin to rise after flow loop transport	≈10.00
Core Inlet Mass Flux begins to lower due to lower density of coolant	≈10.00
MDNBR estimated to reach Low DNBR reactor trip setpoint	<30.00
Reactor Trip Setpoint reached (Low Saturation Margin/Low Primary Pressure)	59.454
Reactor Trip	60.435
Turbine Trip	61.035
Safety Bank Scram Rods fully inserted	64.335

Figure 26-1—Fraction of Power versus Transient Time for BOC REA

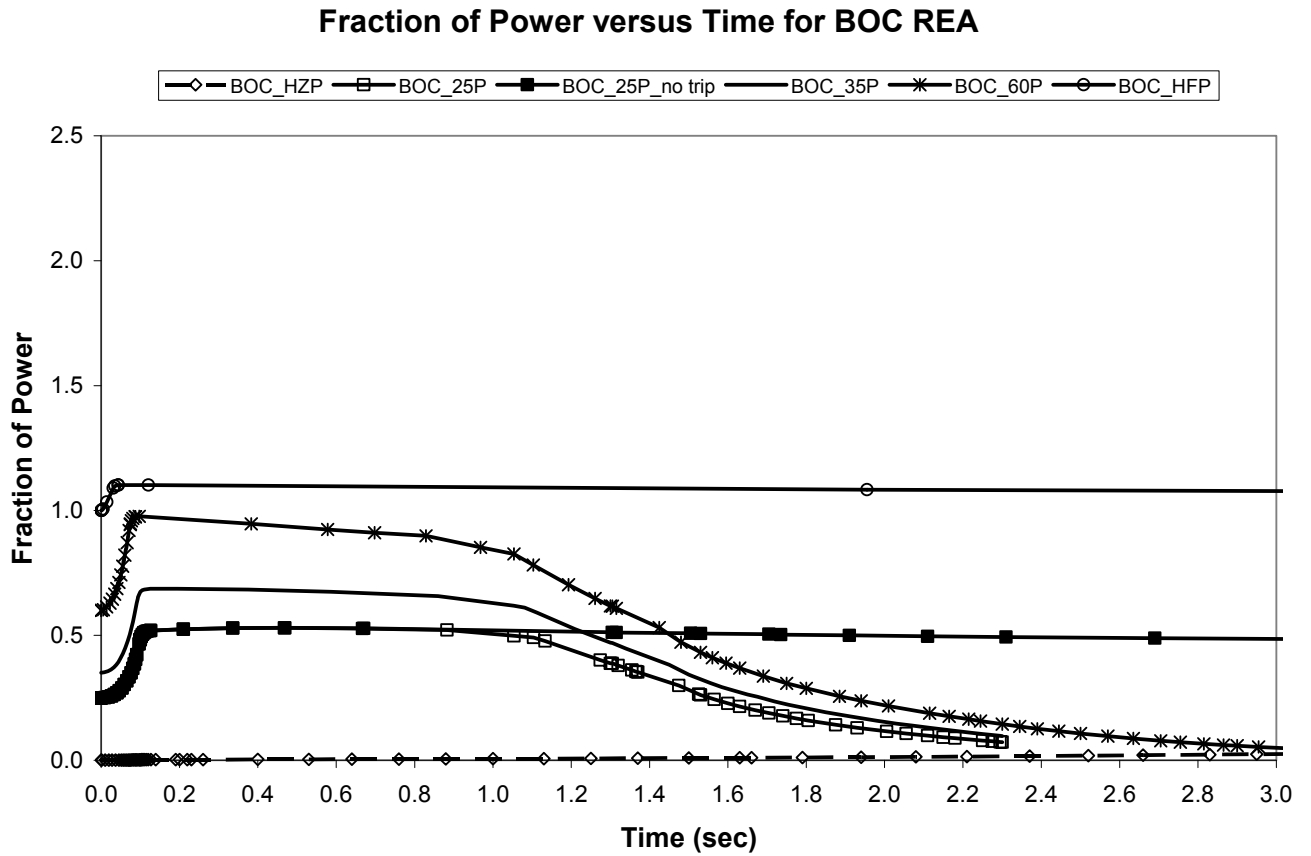


**Figure 26-2—Fraction of Power versus Transient Time for EOC REA**

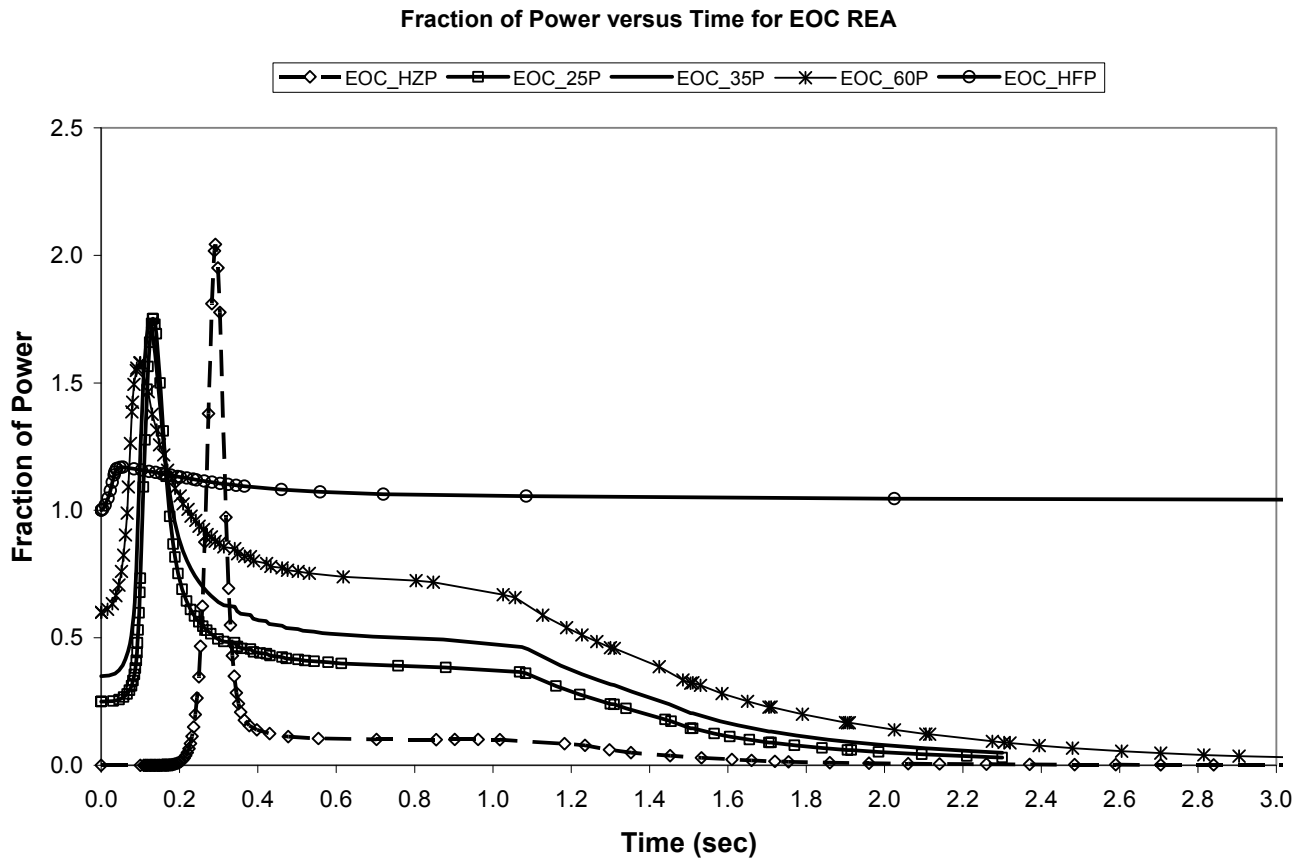


**Figure 26-3—S-RELAP5 Normalized Boundary Conditions for 25 percent  
power BOC Rod Ejection**



**Figure 26-4—S-RELAP5 Normalized Boundary Conditions for BOC HFP  
Rod Ejection**



**Figure 26-5—Pressure and Temperature Conditions for BOC HFP  
S-RELAP5 Case and MDNBR=1.8**



*RAI-27. Provide a description of the thermal properties tables' inputs to LYNXT.*

**Response to RAI-27:**

The fuel rod thermal properties tables that are input to LYNXT for the LYNXT Constant Gap/Temperature Dependent Properties (CG/TDP) option are input as pairs of temperatures and thermal property value at that temperature. The properties are the fuel thermal conductivity, fuel specific heat, cladding thermal conductivity, and cladding specific heat. The gap conductance property is input as a [

]. Additionally, the fuel enthalpy can be input as a function of fuel temperature in order for LYNXT to determine the total enthalpy and change in enthalpy at the radial locations in the fuel pellet. The attribute of the radial pellet power profile is input as a function of radial position. The radial power shape is an important attribute for determining the steady state and transient temperature distributions at different burnup conditions. The response to RAI-16 further describes the values in the thermal properties tables used to determine the COPERNIC computer code for the U.S. EPR fuel types.



[  
  
]

### Example Calculation

[ ] assemblies are used to represent the range of radial/axial power behavior during the transient. These assemblies are chosen over a range of [ ] with the corresponding highest [ ]. Assemblies [ ] are chosen for the fuel rod failure census. The [ ] for these assemblies are shown in Figure 28-1. In this BOC HFP example, the N05 fuel assembly has the highest [ ].

The transient power histories for the chosen assemblies/rods, including appropriate uncertainties, are analyzed with the thermal-hydraulic code LYNXT. The power versus time response of the assembly is iteratively scaled up or down by a multiplier until the DNBR reaches the design limit. The multipliers determined for the [ ] fuel assemblies of this example are provided in Table 28-1. For this example, the data in the column labeled "Multiplier" in Table 28-1 are the multipliers for the respective assemblies. For example, any fuel rod that has a pre-ejection  $F_{\Delta H} \geq [ 1.473 ]$  that has a transient power history shape like assembly [ ] will fail. A similar relationship applies to the [ ] fuel assemblies.

[

] The values for the fuel assemblies used in the example are provided in Table 28-2. These multipliers behave linearly as shown in Figure 28-4. Since both correlations are linear, interpolation between the initial  $F_{\Delta H}$  values can be used to obtain the  $F_{\Delta H}$  or  $F_Q$  that would fail the fuel rod.

The pre-ejection fuel rod power is available for fuel rods in the core from the static calculation. The static post ejection failure limit for  $F_{\Delta H}$  and  $F_Q$  are interpolated from the [ ] available values. If the fuel rod has a post ejection  $F_{\Delta H}$  or  $F_Q$  greater than equal to the respective limit interpolated from its initial  $F_{\Delta H}$ , the fuel rod is assumed failed. This process is repeated for each analyzed power level. For the BOC HFP case, the number of pins estimated to be below the MDNBR design limit in the first few seconds of the transient (prompt response) was 0.3 percent.

For the cases that do not trip, as in the HFP BOC case, the core continues to operate in a near steady state neutronic condition so that a failure census is needed to account for the system degradation with time. The pressure slowly degrades due to primary coolant leakage through the assumed hole left by the ejected rod. Since this is a near steady state neutronic problem, the initial power distribution is no longer relevant; only the current power distribution contributes to the heat flux. The process of finding the  $F_{\Delta H}$  and  $F_Q$  values that exceed the DNBR limit is repeated with LYNXT based on the pressure, flow, and inlet temperature provided by S-RELAP5 and the steady state peaking from NEMO-K. For the HFP static case at BOC, the peak assembly power is scaled in LYNXT until it reaches the MDNBR design limit. The values of  $F_{\Delta H}$  and  $F_Q$  for this case become the failure criteria for each rod in the core. Any pin exceeding the  $F_{\Delta H}$  or  $F_Q$  failure criteria is assumed failed. The number of pins estimated to be below the DNBR design limit was 7.2 percent.

**Table 28-1—BOC\_HFP Example Fuel Failure Census  $F_{\Delta H}$  Threshold Determination**



**Table 28-2—BOC\_HFP Example Fuel Failure Static Post-ejection  $F_{\Delta H}$  and  $F_Q$  Threshold Determination**



Where:

- mult =  $F_{\Delta H}$  multiplier factor from Table 28-1 that brings the fuel rod to the MDNBR SAFDL
- fdh0 = initial maximum  $F_{\square H}$  of fuel rods in the selected fuel assembly
- fdh1 = post-ejection maximum  $F_{\square H}$  of fuel rods in the selected fuel assembly
- fq1 = post-ejection maximum  $F_Q$  of fuel rods in the selected fuel assembly

**Figure 28-1—Transient Versus Static Peaking Ratios at 0.150 Seconds**



**Figure 28-2—Transient Versus Static Peaking Ratios at 0.044 Seconds**



**Figure 28-3—Transient Versus Static Peaking Ratios at 0.250 Seconds**



**Figure 28-4—Post Ejection Static DNBR Peaking Limits**



**RAI-29.** *Provide an explanation about the calibration for the high rate flux trip and provide a sample response of the rate lagged filter. (Section 6.2.1, 6.2.1.2, Table 8-1).*

**Response to RAI-29:**

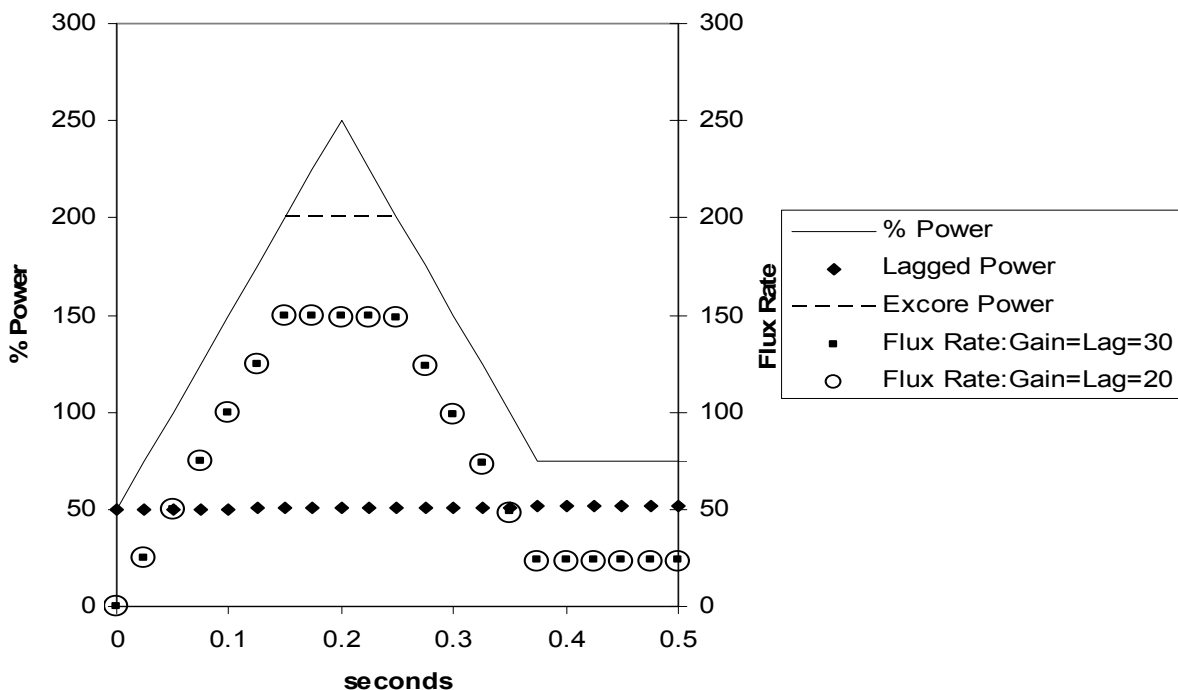
The high flux rate trip is described in U.S. EPR FSAR Tier 2, Section 7.2.1.2.3. The high flux rate is determined from the excore power range detection system signal which is described in U.S. EPR FSAR Tier 2, Section 7.1.1.5.3. The general calibration procedure and surveillance requirement is described in U.S. EPR FSAR Tier 2, Chapter 16, Section 3.3.1. The high rate flux trip is a fixed setting and is not calibrated. The flux rate signal is calculated by the digital protection system using excore detector signal. The definitions and equations in TR Sections 6.2.1.1 and 6.2.1.2 implemented in NEMO-K allow the simulation of these excore protection systems. A calibration is simulated in NEMO-K at the conditions to initialize the indicated power and imbalance of the top and bottom detectors for the four excore detectors. This is done prior to the transient initiation.

Signal filter responses for a fast and normal ramp rate are shown in Figure 29-1 and Figure 29-2, respectively. The figures show the core power, the lagged power, and the flux rate trip signal versus time for a linear ramp increase and decrease in power. The fast ramp rate simulated in Figure 29-1 is 1%/msec and the normal ramp rate in Figure 29-2 is 10%/minute.

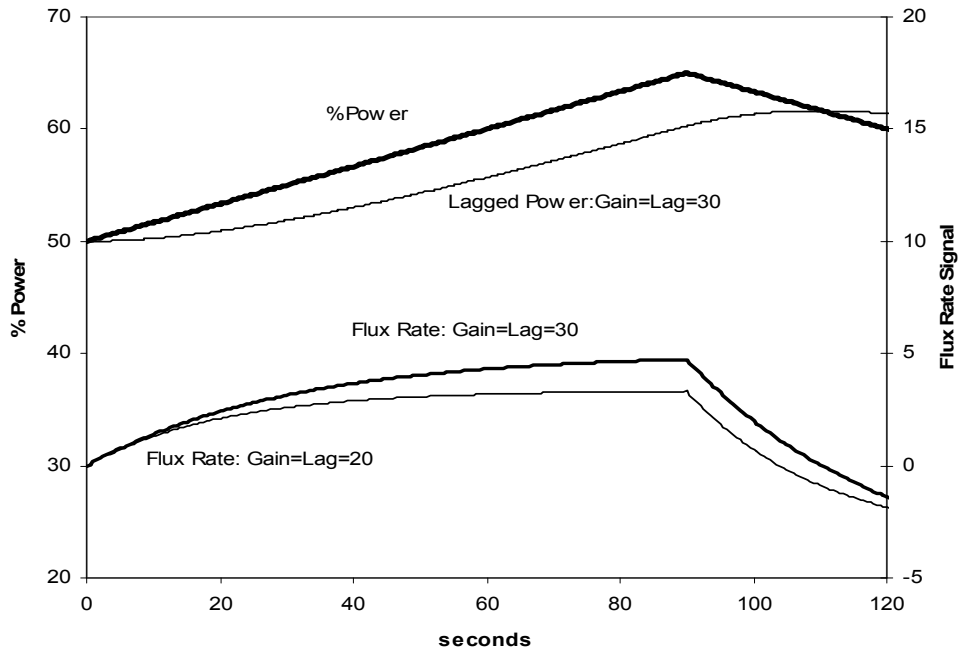
For the fast ramp rate, each point represents a sampling rate of once every 25 milliseconds. The fast ramp rate illustrates the signal response during a prompt excursion. The excore power will indicate no higher than 200 percent power when the actual power is above 200 percent power. For the fast ramp rate figure, the flux rate signal is nearly equal to the delta power observed from  $t=0$  because the lagged power signal does not change in this short time frame relative to the 30 second lag time. The flux rate signal remains high throughout the transient even though the power is going down. The flux rate values for 20 second gain and lag constants is indistinguishable from the values with 30 second time constants. The label of normal ramp rate corresponds to a 10%/minute ramp rate, which is a relatively fast maneuvering rate. Figure 29-2 shows an asymptotic 5 percent rate signal, which agrees with the ramp rate (10%/60 seconds) times the gain constant (30). The flux rate signal with the gain and lag set to 20 reaches its maximum value of 3.3 (10%/60 seconds times 20) more quickly than the gain and lag set to 30.

Figure 29-3 and Figure 29-4 show the core power and the flux rate trip signal for each excore detector versus time for the BOC HFP and EOC HZP transient simulations, respectively. As shown in Figure 29-3 for the BOC HFP ejected rod transient, only one of the four flux rate signals exceeded the trip limit and the reactor did not trip. The highest detector response is the detector location closest to the ejected rod. In Figure 29-4 for the EOC HZP ejected rod transient, each point represents a sampling rate of once every 25 ms and three detectors indicated a trip signal twice leading to a trip signal being activated.

**Figure 29-1—Flux Rate Signal Fast Ramp Rate**



**Figure 29-2—Flux Rate Signal – Normal Ramp Rate**



**Figure 29-3—BOC HFP – Flux Rate Signals**

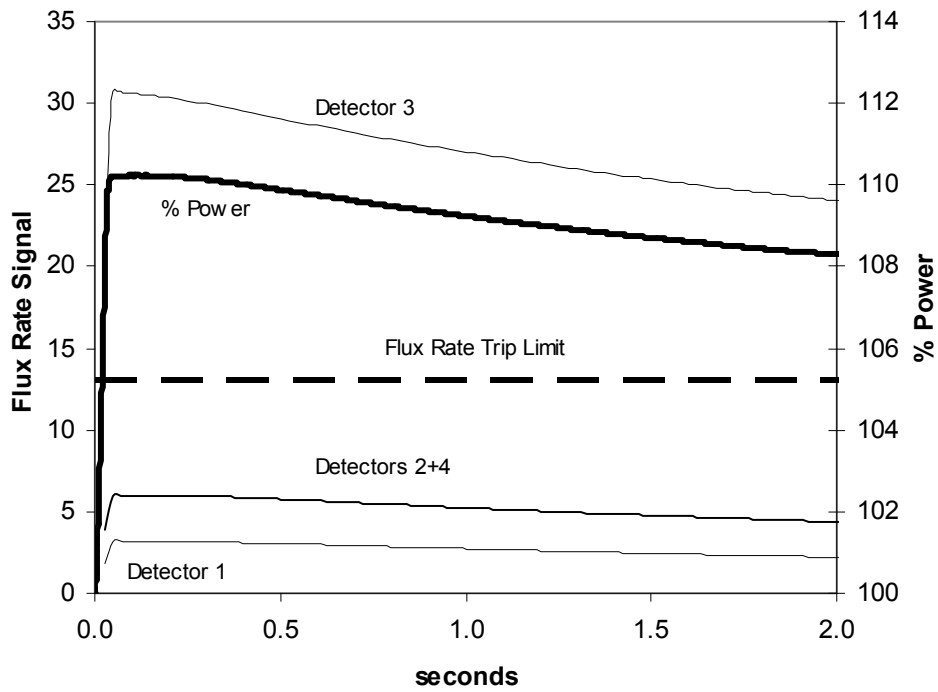
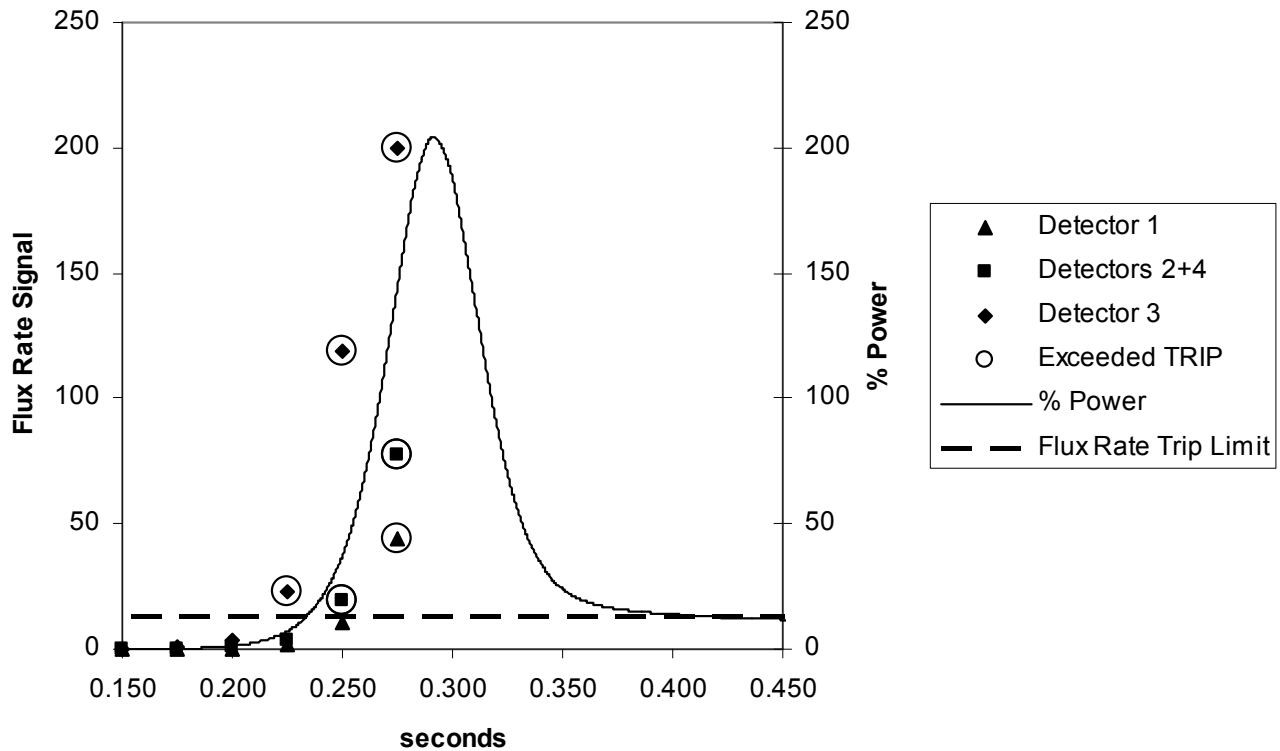


**Figure 29-4—EOC HZP – Flux Rate Signals**



**RAI-30.** Section 7.2.4 – Please explain why the assembly pin power radial power distribution in LYNXT is conservative for the assumed power distribution within the fuel assembly of interest.

**Response to RAI-30:**

The radial power distribution for the sample problem fuel rods is based on the distribution used in other MDNBR analyses for the U.S. EPR (e.g., U.S. EPR FSAR Tier 2, Chapter 15 events).

[

] The power distribution selected for DNBR analysis was based on investigations of the fuel assembly lattice fuel rod power distribution from several cycles and burnups. The power distribution used for the U.S. EPR analysis is presented in Table 30-1. As described in TR Section 7.2.4, [

] The equation to provide the proper core normalized  $F_{\Delta H}$  for the last [ ] nodes is provided in TR Section 7.2.4.

**Table 30-1—Relative Power Factors for LYNXT Model Fuel Rod Nodes**



**RAI-31.** *Please provide an explanation for the discontinuities of the LYNXT results relative to the COPERNIC temperature transients in Figures 6-23 and 6-27.*

**Response to RAI-31:**

The discontinuities of the LYNXT results in TR Figures 6-23 and 6-27 are related to the interpolation for the value of the gap conductance from the table values input as part of the CG/TDP option. The model assumptions for LYNXT and COPERNIC are described in the response to RAI-24. For LYNXT, the gap conductance (HGAP) input is a [ ] The format of the HGAP property set is described in the response to RAI-16. The fuel average temperature and HGAP values from LYNXT and COPERNIC are shown in Figure 31-1. The fuel temperatures are the same as the values shown in TR Figure 6-24. During the transient, the average [ ] temperature is maintained between [ ], which are [ ] index into the HGAP table. The fuel average temperature transitions from [ ] during the [ ] seconds of the simulation. Also indicated in Figure 31-1 are the time points of the [ ]

[ ] The fuel temperatures transition through [ ]

[ ] These are the times at

which the temperature cusping inflections occur in Figure 31-1 and in TR Figures 6-23 and 6-27. The slope of the HGAP changes at these points; therefore, the response in LYNXT will be affected.

During the transient, the LYNXT fuel surface temperatures in TR Figure 6-23 are at most [ ] °F lower and at the [ ] second end of transient, the LYNXT value is approximately [ ] °F higher than the COPERNIC value. Because the HGAP value is [ ] in the LYNXT results than in the COPERNIC results, during the initial phases of the transient, the heat flux from the fuel rod will be [ ], the fuel surface will tend to be [ ], and the cladding maximum temperature will tend to be [ ]. This is shown in TR Figure 6-27.

While developing the response to RAI-31, a typographical error was found in the input for LYNXT gap conductance for the BOL cases. The input typo resulted in the HGAP for [ ] being set to an incorrect low value. The LYNXT calculations were re-run and the correct results once again compared to the COPERNIC results. The change in the results of the LYNXT transient occur only after [ ] seconds and results in changes less than [ ] percent (i.e., [ ] °F) in fuel and clad temperatures and changes less than [ ] percent ( [ ]) for the temperature ratios for the HFP BOL case in TR Table 6-3. The maximum ratio of the cladding maximum temperature changed from [ ]. The minimum ratio for the fuel surface temperature changed from [ ] and for the average fuel temperature changed from [ ]. The rest of the ratios in the table remained the same. A revised TR Table 6-3, TR Figure 6-23, and TR Figure 6-27 are provided in the attachment to this RAI response. The above error was also documented in the AREVA corrective action program.

**Figure 31-1—LYNXT and COPERNIC Fuel Average Temperature and Gap Conductance for Comparison Model REA from HFP/BOC**



**RAI-32.** *Please explain why the BOC HZP was not analyzed in LYNXT in Sections 8.1 and 8.3*

**Response to RAI-32:**

The BOC HZP power case was not analyzed for MDNBR response in LYNXT because the power response at HZP BOC changes less than 6 percent power from 0 to 5 seconds, as shown in TR Figure 8-1. In TR Figure 8-2, the power response at BOC for 25 percent power increases more than 25 percent power in less than 0.2 seconds and clearly bounds the changes seen at HZP BOC. Because the ejected rod reactivity worth is less than the effective delayed neutron fraction  $\beta_{\text{eff}}$ , the power rise is caused by the prompt jump in reactivity and is not a prompt critical excursion. The prompt jump is a fractional change of the initial power so that a higher initial power results in a higher change in power. Therefore, the BOC HZP case was not analyzed with LYNXT because it was bounded by the conditions at 25 percent power. To indicate that the BOC HZP case was not analyzed beyond the neutronic calculation, the number of fuel rods failed in TR Table 8-4 at 0 percent power should be labelled with a dash rather than a value of 0 indicating that the results are bounded by the results at 25 percent power. A marked up revision to TR Table 8-4 is provided in the attachment to this RAI.

# ANP-10286 Markups

**Table 6-3 LYNXT and COPERNIC Transient Temperature Ratio Comparisons**

Comparison parameter	Fuel temperature				Cladding maximum temperature
	Surface	Average	Centerline	Maximum	
<b>HZP EOL</b>					
Average					
Std. dev.					
Maximum					
Minimum					
Sample size					
<b>HFP EOL</b>					
Average					
Std. dev.					
Maximum					
Minimum					
Sample size					
<b>HZP BOL</b>					
Average					
Std. dev.					
Maximum					
Minimum					
Sample size					
<b>HFP BOL</b>					
Average					
Std. dev.					
Maximum					
Minimum					
Sample size					

Notes:

1. The data is based on (COPERNIC result) / (LYNXT CG/TDP result).
2. "Std. dev." is the standard deviation of the data about the average. Sample size is the number of transient time steps.

**Figure 6-23 HFP/BOL Transient Fuel Surface Temperature**



**Figure 6-24 HFP/BOL Transient Fuel Average Temperature**



**Figure 6-27 HFP/BOL Transient Cladding Maximum Temperature**



burnup for a 2.0 and 5.0 w/o U-235 pellet is estimated to be 50 and 70 GWD/MTU, respectively. The MDNBR performance is shown in Figure 7-9 for these cases. [

] This is

due to higher gap conductance values and higher pellet rim power peaking.

Calculations are performed with 5.0 w/o U-235 fuel at 2.5 and 50 GWD/MTU burnup levels for the BOC cases and 20 and 70 GWD/MTU burnup levels for the EOC cases in order to bound the potential burnup thermal property states of the fuel rods.

Fuel loaded with gadolinia has a lower thermal conductivity than pure  $\text{UO}_2$ . The higher the gadolinia content, the lower the thermal conductivity of the fuel pellet. This increases the fuel temperatures of the gadolinia fuel if operated at the same LHGR as a  $\text{UO}_2$  fuel rod. However the gadolinia rods typically have low maximum powers because of lower fuel uranium enrichments and parasitic neutron absorption by the residual gadolinium isotopes. To determine if the analysis can be performed using only  $\text{UO}_2$  properties, a sensitivity study was run on the BOC HFP power excursion with gadolinia loadings of 4 w/o and 8 w/o gadolinia. The gadolinia rods were run with the same power history as the pure  $\text{UO}_2$  rod and with the maximum power level anticipated for a gadolinia loaded rod. [

] Figure 7-10

shows the peak fuel temperatures for 0, 4, and 8 w/o gadolinia loadings. Note that the fuel temperatures with gadolinia are higher when operating at the same linear heat rate as  $\text{UO}_2$ . ~~and~~ When the transient temperatures for gadolinia fuel are adjusted by the power reduction factor, are the maximum temperature during the transient is bounded by the  $\text{UO}_2$  maximum temperatures. For the thermally limiting transient for HFP at BOC, the temperatures never exceed the lowest fuel melt limit for a rim burnup, even when the peak power is not decreased by the maximum expected value for a gadolinia rod. Because the  $\text{UO}_2$  rod bounds the temperatures, the LYNXT calculations use the

[

]

**Table 8-4 Ejected Rod Analysis Results for BOC**

Parameter	Criterion	0	25	35	60	100
Maximum Ejected Rod Worth, pcm	-	433	362	346	286	64
$\beta_{\text{eff}}$	-	0.0055	0.0055	0.0055	0.0055	0.0055
MTC, pcm/°F	-	2.16	1.32	1.35	0.34	0.01
DTC, pcm/°F	-	-1.22	-1.14	-1.11	-1.05	-0.96
Initial $F_Q$	-	NA <sup>a</sup>	3.01	2.88	2.63	2.36
Maximum Transient $F_Q$	-	9.46	5.75	5.23	5.06	2.70
Initial $F_{\Delta H}$	-	NA <sup>a</sup>	2.15	2.09	1.94	1.70
Maximum Transient $F_{\Delta H}$	-	5.21	3.75	3.58	3.01	2.11
Maximum Neutron Power, FOP	-	0.32	0.55	0.69	0.98	1.10
Maximum cal/g	$\leq 150$	-	70.4	50.4	63.9	109.4
Maximum $\Delta\text{cal/g}$ , prompt	$\leq 110$	-	10.0	10.9	11.8	7.2
Maximum Fuel Temperature, °F	[       ]	-	2655	1901	2529	4014
Maximum Cladding Temperature, °F	[       ]	-	1098	727	951	1461
MDNBR/SAFDL Ratio For Failure	$\leq 1.0$	-	0.71	1.86	0.96	0.33
Time of Trip (initiation of safety bank insertion), seconds	-	No Trip	No Trip <sup>b</sup>	0.850	0.825	No Trip
Equivalent nominal rods failed, %	$\leq 30$	0	1.8	0	0	7.2

## Notes:

<sup>a</sup> Not applicable since initial stored energy above the coolant temperature is zero.

<sup>b</sup> Trip is disabled to bound consequences of powers lower than 25%.